Journal of Computational Physics 230 (2011) 1198–1214

Contents lists available at ScienceDirect

Journal of Computational Physics

journal homepage: www.elsevier.com/locate/jcp

# Nonlinear variants of the TR/BDF2 method for thermal radiative diffusion

Jarrod D. Edwards [a], Jim E. Morel [a,*], Dana A. Knoll [b]

[a] Department of Nuclear Engineering, 129 Zachry Engineering Center, TAMU 3133, Texas A&M University, College Station, Texas 77843, USA
[b] Fluid Dynamics and Solid Mechanics Group T-3, Los Alamos National Laboratory, P.O. Box 1663, MS B216, Los Alamos, NM 87545, USA

ARTICLE INFO

*Article history:*
Received 27 April 2010
Received in revised form 22 October 2010
Accepted 27 October 2010
Available online 11 November 2010

*Keywords:*
Trapezoidal BDF-2
nonlinear radiative diffusion

ABSTRACT

We apply the Trapezoidal/BDF2 (TR/BDF2) temporal discretization scheme to nonlinear grey radiative diffusion. This is a scheme that is not well-known within the radiation transport community, but we show that it offers many desirable characteristics relative to other second-order schemes. Several nonlinear variants of the TR/BDF2 scheme are defined and computationally compared with the Crank–Nicholson scheme. It is found for our test problems that the most accurate TR/BDF2 schemes are those that are fully iterated to nonlinear convergence, but the most efficient TR/BDF2 scheme is one based upon a single Newton iteration. It is also shown that neglecting the contributions to the Jacobian matrix from the cross-sections, which is often done due to a lack of smooth interpolations for tabular cross-section data, has a significant impact upon efficiency.



## 1. Introduction

The Crank–Nicholson (CN) [1] scheme has been traditionally used in the computational community for second-order accurate radiation transport and diffusion calculations. However, this scheme can yield highly oscillatory solutions for stiff systems. A more accurate, highly damped alternative to Crank–Nicholson is the linear-discontinuous Galerkin (LDG) scheme [2]. Although this scheme has several desirable properties, solving the LDG equations is significantly more computationally intensive than solving the Crank–Nicholson equations. In particular, solving the LDG equations is analogous to solving two CN-like systems simultaneously over each time step. Thus it is a two-stage[1] scheme with implicit coupling between the stages. Furthermore, the LDG method significantly complicates traditional transport iterative convergence acceleration techniques such as diffusion-synthetic acceleration [2]. The second-order backward difference formula (BDF2) [1] is a one-stage scheme that requires solution values from two previous time steps rather than one (a two-step scheme). It is highly damped and compatible with existing transport acceleration techniques. However, as we will later show, the BDF2 scheme has unusual conservation properties that we consider undesirable. It is clear from our discussion that an ideal second-order scheme would possess the following properties:

- one stage,
- one step,
- strong damping of oscillations,
- compatibility with existing transport acceleration techniques,
- standard conservation properties.

* Corresponding author.
*E-mail address:* morel@tamu.edu (J.E. Morel).

[1] Here we use the term "stage" to refer to an implicit equation that must be solved each time step in a discretization scheme, but as explained in Section 3.4, the same term can have a slightly different meaning when referring to Runge–Kutta methods.

0021-9991/$ - see front matter © 2010 Elsevier Inc. All rights reserved.
doi:10.1016/j.jcp.2010.10.035

We are unaware of any scheme that has all of these properties, but the trapeziodal/BDF2 scheme (TR/BDF2) [6] has all but one. It is a two-stage scheme. However, unlike the LDG method, the TR/BDF2 scheme requires two sequential CN-like solves rather than two coupled CN-like solves. Thus the TR/BDF2 scheme has lower-triangular coupling between the two stages, i.e., the first stage does not depend upon the second stage, but the second stage uses information from the first stage The purpose of this paper, is to analyze the order, damping, and conservation properties of the TR/BDF2 method, and apply it to the 1D, grey equations of nonlinear radiative heat diffusion. Because these equations are nonlinear, we also examine various treatments for the nonlinear terms. Traditionally, the Newton method is used to solve these equations. However, because photon cross-section data is generally tabular, the contributions to the Jacobian matrix from the cross sections are usually neglected, resulting in a kind of hybrid Newton–Picard method. We examine the cost of the Newton–Picard method in terms of both accuracy and efficiency relative to the pure Newton method. We also compare the efficiency obtained by converging the nonlinear terms with that obtained by fixing the number of iterations. The study presented here is somewhat similar to that of Lowrie [3] except that he considered variations of the Crank–Nicholson scheme rather than the TR/BDF2 scheme.

In the remainder of the paper, we describe the TR/BDF2 scheme and demonstrate some of its important properties. We then develop our variants on the scheme which we later apply to the radiative heat diffusion equations. We describe the two problems we use to test our methods – a smooth, sinusoidal problem and a Marshak wave, and show the results for each before presenting our conclusions.

## 2. Radiative heat diffusion equations

The radiative heat diffusion equations (RHDEs) describe how heat is exchanged via photon emission and absorption with the assumption that the angular distribution of the radiation is linear. We further assume a 1D, grey model for radiation energy density and material temperature. Thus, the RHDEs are:

$$\frac{\partial E}{\partial t} - \frac{\partial}{\partial x}\frac{c}{3\sigma_t}\frac{\partial E}{\partial x} = \sigma_a c(aT^4 - E), \tag{1}$$

$$C_v\frac{\partial T}{\partial t} = \sigma_a c(E - aT^4). \tag{2}$$

The dependent variables in these equations, $E$ and $T$, represent radiation energy density and material temperature, respectively. The absorption and total cross-sections, $\sigma_a$ and $\sigma_t$, both strongly depend on temperature, but because the heat capacity, $C_v$, only weakly depends on $T$, we treat it as constant. Lastly, $a$ and $c$ represent the Boltzmann constant and the speed of light. In space, these equations are discretized using an LDG scheme, which is second-order accurate. [4,5] These equations are solved by first linearizing Eqs. (1) and (2) using one of two methods described in a later section. Then, the linearized version of Eq. (2) is used to eliminate the implicit temperature terms from Eq. (1) resulting in a diffusion equation implicitly dependent only on $E$. Due to the relatively few number of unknowns used in our problems, this equation is solved directly using Gauss elimination. Finally, using $E$ and Eq. (2), the temperature is computed locally.

## 3. TR/BDF2 method

The TR/BDF2 method was developed by Bank et al. [6]. It is a one step algorithm in which the solution is computed over a portion of the time step, $\gamma\Delta t$, using the Trapezoid Rule (Crank–Nicholson method). Then, the solution over the remainder of the time step, $(1-\gamma)\Delta t$, is computed using the BDF2 method. Consider the following nonlinear equation:

$$\frac{\partial f}{\partial t} = \mathbf{A}f, \tag{3}$$

where $f$ is the solution and $\mathbf{A}$ is a nonlinear operator dependent on $f$. The general TR/BDF2 scheme may be written as:

$$\frac{f^{n+\gamma} - f^n}{\gamma\Delta t} = \frac{1}{2}(\mathbf{A}^{n+\gamma}f^{n+\gamma} + \mathbf{A}^n f^n), \tag{4a}$$

$$\frac{(2-\gamma)f^{n+1} - \gamma^{-1}f^{n+\gamma} + \gamma^{-1}(1-\gamma)^2 f^n}{\Delta t} = (1-\gamma)\mathbf{A}^{n+1}f^{n+1}. \tag{4b}$$

Bank demonstrated that the optimum value of $\gamma$ is $\sqrt{2}-2$; however, for simplicity, we use $\gamma = 1/2$. Thus, Eqs. (4a) and (4b) become:

$$\frac{2(f^{n+1/2} - f^n)}{\Delta t} = \frac{1}{2}(\mathbf{A}^{n+1/2}f^{n+1/2} + \mathbf{A}^n f^n), \tag{5a}$$

$$\frac{3f^{n+1} - 4f^{n+1/2} + f^n}{\Delta t} = \mathbf{A}^{n+1}f^{n+1}. \tag{5b}$$

We later demonstrate that any advantages in accuracy and stability of the optimal scheme relative to our simplified scheme are negligible.

### 3.1. Conservation

The analytic average value of $\mathbf{A}f$ over a time step is only a function of $\mathbf{A}f$ values evaluated within that step. To demonstrate that a conservation statement may be made for the TR/BDF2 scheme over a single time step, we multiply Eq. (5a) by 2, add it to Eq. (5b) and divide the sum by 3 to get the following:

$$\frac{f^{n+1}-f^n}{\Delta t}=\frac{1}{3}(\mathbf{A}^{n+1}f^{n+1}+\mathbf{A}^{n+1/2}f^{n+1/2}+\mathbf{A}^n f^n). \tag{6}$$

From Eq. (6), we see that the average time derivative of the solution over one time step is equal to an uniform three-point average of $\mathbf{A}f$ over the same time step. Let us now compare this with the BDF2 scheme described in Section 1. We demonstrate that the BDF2 scheme fails to preserve this analytic property due to the fact that it is a multistep scheme. One step schemes, like the TR/BDF2 method, have no knowledge of solution values that lie outside of any given time step; thus, additional values cannot appear in the conservation expression. For this demonstration, we use a fixed time step for simplicity, but the principles we demonstrate apply with arbitrary time steps. Because the BDF2 scheme is a two-step method, we must use an one-step scheme to determine the first time step. Here, we use the Crank–Nicholson scheme. Thus, the solution over the first step is computed using:

$$\frac{f^{(1)}-f^{(0)}}{\Delta t}=\frac{1}{2}(\mathbf{A}^{(1)}f^{(1)}+\mathbf{A}^{(0)}f^{(0)}). \tag{7}$$

Then, using the standard BDF2 scheme, the solution can be computed at each subsequent time:

$$\frac{3}{2}\frac{f^{n+1}-f^n}{\Delta t}-\frac{1}{2}\frac{f^n-f^{n-1}}{\Delta t}=\mathbf{A}^{n+1}f^{n+1}. \tag{8}$$

The partial time derivative of $f$ averaged over $[t^n,t^{n+1}]$ can be expressed for the BDF2 scheme as follows:

$$\frac{f^{n+1}-f^n}{\Delta t}=\frac{1}{3}\frac{f^n-f^{n-1}}{\Delta t}+\frac{2}{3}\mathbf{A}^{n+1}f^{n+1}. \tag{9}$$

Using Eqs. (9) and (7), we find that the conservation expression for the second time step may be written as:

$$\frac{f^{(2)}-f^{(1)}}{\Delta t}=\frac{4}{6}\mathbf{A}^{(2)}f^{(2)}+\frac{1}{6}\mathbf{A}^{(1)}f^{(1)}+\frac{1}{6}\mathbf{A}^{(0)}f^{(0)}. \tag{10}$$

Note from the above equation that $\mathbf{A}^{(0)}f^{(0)}$ plays a role in the conservation expression over the time step from $t^{(1)}$ to $t^{(2)}$. Using Eqs. (9) and (10), we obtain the conservation expression for the third step:

$$\frac{f^{(3)}-f^{(2)}}{\Delta t}=\frac{12}{18}\mathbf{A}^{(3)}f^{(3)}+\frac{4}{18}\mathbf{A}^{(2)}f^{(2)}+\frac{1}{18}\mathbf{A}^{(1)}f^{(1)}+\frac{1}{18}\mathbf{A}^{(0)}f^{(0)}. \tag{11}$$

It is not difficult to see from these examples that continued application of Eq. (9) yields a conservation statement at each time step that depends upon values of $\mathbf{A}f$ evaluated at each and every previous time. Thus while a conservation expression for each time step can be made with the BDF2 scheme, the resulting expression has an undesirable dependence upon all previously computed values of $\mathbf{A}f$. Nevertheless, if one wishes to compute a conservation statement for the BDF2 scheme for each time step, it can be done fairly efficiently. For instance, if one is only interested in the average value of $\mathbf{A}f$ over the time step, Eq. (9) can be directly used. However, it is often of interest to decompose the average of $\mathbf{A}f$ into a sum of component source rates and sink rates. Examples of such components for radiation diffusion include the radiation energy absorption, emission, inflow, and outflow rates. Eq. (9) cannot be directly used to compute such components because one does not know how to decompose the terms on the right side of that equation that are functions of $f$ rather than $\mathbf{A}f$. This problem can be circumvented by recognizing that Eq. (9) is a recursion formula that relates successive averages of $\mathbf{A}f$. In particular, we can re-express Eq. (9) as follows:

$$\langle\mathbf{A}f\rangle^{n+\frac{1}{2}}=\frac{1}{3}\langle\mathbf{A}f\rangle^{n-\frac{1}{2}}+\frac{2}{3}\mathbf{A}^{n+1}f^{n+1}, \tag{12}$$

where $\langle\mathbf{A}f\rangle^{n+\frac{1}{2}}$ denotes the average value of $\mathbf{A}f$ from $t^n$ to $t^{n+1}$. One can directly compute the components of $\overline{\mathbf{A}f}$ for the first time step (which must be performed with an one-step scheme), and then use Eq. (12) to compute the components for each successive BDF2 step. While Eq. (12) only applies with uniform time steps, one can easily compute an analog for arbitrary time steps. The general BDF2 equation for computing $f^{n+1}$ given $f^n$ and $f^{n-1}$ is

$$\left(\frac{2t^{n+1}-t^n-t^{n-1}}{t^{n+1}-t^{n-1}}\right)\left(\frac{f^{n+1}-f^n}{t^{n+1}-t^n}\right)-\left(\frac{t^{n+1}-t^n}{t^{n+1}-t^{n-1}}\right)\left(\frac{f^n-f^{n-1}}{t^n-t^{n-1}}\right)=\mathbf{A}^{n+1}f^{n+1}. \tag{13}$$

### 3.2. Accuracy

Next, to demonstrate accuracy and stability, consider the following ODE:

$$\frac{\partial f}{\partial t} + kf = 0, \quad f(0) = 1, \ k > 0. \tag{14}$$

Applying Eqs. (5a) and (5b) to the ODE in Eq. (14), we get the following solution for $f^{n+1}$:

$$f^{n+1} = \frac{12 - 5z}{12 + 7z + z^2} f^n. \tag{15}$$

where $z = k\Delta t$. By performing a Taylor series expansion on Eq. (15) and comparing that with a Taylor series expansion of the exact solution, $f(t) = exp(-z)$, we see that the expression in Eq. (15) is locally third-order accurate:

$$f^{n+1} = e^{-z} - \frac{1}{24}(z^3). \tag{16}$$

Thus, the method is globally second-order accurate. The leading-order coefficient for the optimal TR/BDF2 method is $-\left(\frac{1}{\sqrt{3}} - \frac{2}{3}\right) \approx -0.0404$ which is negligibly smaller in magnitude than $-\frac{1}{24} \approx -0.0417$. Thus the difference in truncation error between the two methods is negligible.

### 3.3. Stability

As shown in Fig. 1, by plotting the amplification factor that relates $f^n$ to $f^{n+1}$ in Eq. (15), we can observe the stability of the method as a function of $z$. We can see that the function has a maximum value of 1, a minimum value of −0.212, and approaches zero as $z$ approaches infinity; thus, the TR/BDF2 method is L-stable. Furthermore, though the method can oscillate, oscillatory modes will be damped by about 80% at each time step. This is much better behavior than the Crank–Nicholson scheme, which is not L-stable and has a minimum value of −1 so that oscillatory modes may not be damped at all. The optimal TR/BDF2 method has a minimum amplification factor of −0.207, which is negligibly better than that of the simplified TR/BDF2 value.

### 3.4. Connection to Runge–Kutta methods

The general TR/BDF2 scheme can be categorized as an implicit Runge–Kutta method. For instance, an $s$-stage Runge–Kutta method for solving the nonlinear equation

$$\frac{\partial f}{\partial t} = G(t, f), \tag{17}$$

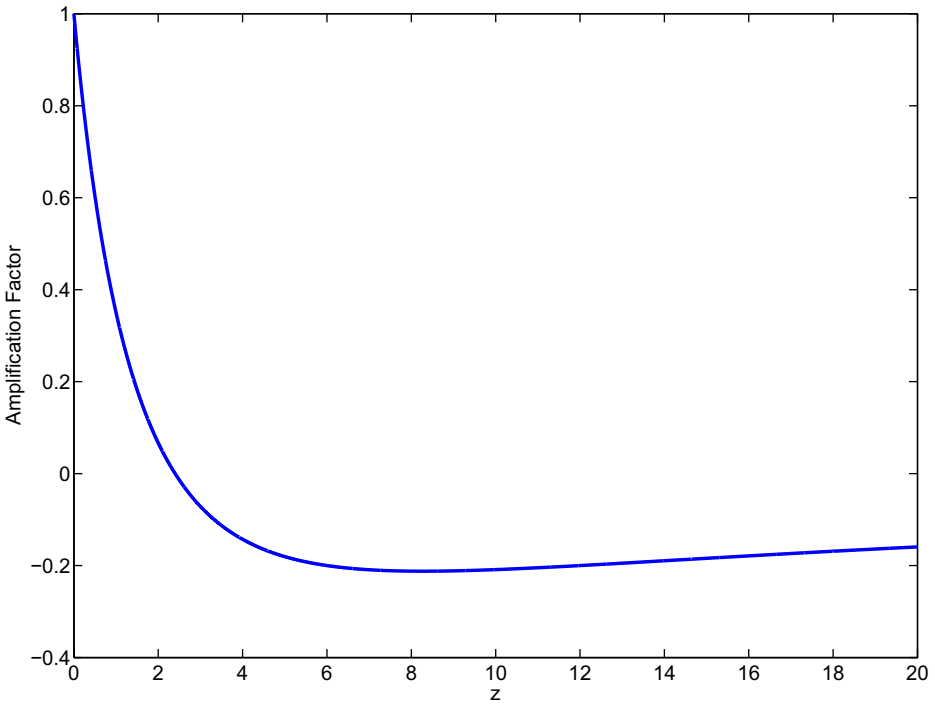


**Fig. 1.** Stability curve for the TR/BDF2 scheme.

can be expressed in terms of the $s \times s$ matrix $B$, and the $s$-vectors $c$ and $d$ as follows:

$$F_i = f^n + \Delta t \sum_{j=1}^{s} b_{ij} G(t^n + c_j \Delta t, F_j), \quad i = 1, \ldots, s, \tag{18}$$

$$f^{n+1} = f^n + \Delta t \sum_{i=1}^{s} d_i G(t^n + c_i \Delta t, F_i). \tag{19}$$

This information can be conveniently expressed using a Butcher coefficient tableau [7]:

$$\begin{array}{c|c} \mathrm{c} & \mathrm{B} \\ \hline & \mathrm{d}^T. \end{array} \tag{20}$$

The tableau for the general TR/BDF2 scheme (which requires considerable algebraic manipulation of Eqs. (4a) and (4b) to obtain) is

$$\begin{array}{c|ccc} 0 & 0 & 0 & 0 \\ \gamma & \gamma/2 & \gamma/2 & 0 \\ 1 & 1/[2(2-\gamma)] & 1/[2(2-\gamma)] & (1-\gamma)/(2-\gamma) \\ \hline & 1/[2(2-\gamma)] & 1/[2(2-\gamma)] & (1-\gamma)/(2-\gamma) \end{array} \tag{21}$$

Note from the tableau that this scheme has three stages. However, because $F_1$, is equal to $f^n$ one need not solve an equation to obtain it. Schemes with this property are referred to as FSAL (First-Same as Last). In Section 1 we defined the number of stages in a scheme as the number of equations that have to be solved over a time step. This is equivalent to the number of Runge–Kutta stages for all but FSAL schemes. In Section 1 we noted that the two equations that must be solved each time step in the general TR/BDF2 method can be solved sequentially rather than simultaneously. This property is expressed in the tableau by the lower-triangular structure of $B$. Schemes with this property are referred to as Diagonally-Implicit-Runge–Kutta (DIRK) schemes. If the diagonal elements for all stages associated with the solution of an equation are identical, the scheme is referred to as a Singly-Diagonally-Implicit-Runge–Kutta (SDIRK) scheme [7]. The optimal TR/BDF2 scheme is the only TR/BDF2 scheme that is SDIRK. The significance of this property is that if one is applying the Newton method and uses a single Jacobian over the entire time step (an approximate Newton method), the matrix associated with the linearized equation for each stage will be identical for all stages. This can lead to improved efficiency, but there are several caveats. For instance, the Jacobian-Free-Newton–Krylov method [8], which is becoming increasingly popular for applying the Newton method to very large systems of equations, is equally efficient for DIRK and SDIRK methods. If one is taking relatively large time steps, the approximate Newton method may encounter convergence difficulties. Thus we do not consider the fact that our simplifed TR/BDF2 scheme is DIRK rather than SDIRK to be a significant disadvantage relative to the optimal scheme.

## 4. Variations on the TR/BDF2 method

Here, we describe our variations on the TR/BDF2 scheme. They differ according to our treatment of the cross sections and whether the solution is converged or the number of iterations fixed. To ensure stability, the Planck function is always treated via the Newton method. We treat the cross-sections using two types of iteration schemes. The first is the Newton method, which requires temperature derivatives of the cross-sections and converges quadratically once the iterate is sufficiently close to the solution. [9] The second iteration scheme is Picard's method (also known as fixed-point iteration) which does not require temperature derivatives of the cross sections but converges linearly once the iterate is sufficiently close to the solution. [9] For simplicity, we define our methods in terms of Eq. (3). When it is necessary, the operator $\mathbf{A}$ is expressed as a product of two matrices, $\mathbf{B}$ and $\mathbf{C}$, where the former represents those components of $\mathbf{A}$ containing cross sections and the latter represents those containing the Planck function. Our system cannot actually be expressed in this form, but we assume that it can be so expressed as a simple device for making the treatment of the cross sections and the Planck function apparent without consideration of the full equations. The operators in our descriptions carry iteration information in addition to time indexing. Quantities evaluated at the previous iterate carry a superscript "*". For instance, $f^*$ denotes the previous iterate for $f$. The primary unknown in each equation takes the form of $\delta f$, the additive change in the iterate for $f$. For instance, the new iterate of $f$ is given by $\delta f + f^*$.

### 4.1. Converged newton method

The first variation is to apply the Newton method to both the cross sections and the Planck function.

$$\frac{2(\delta f + f^* - f^n)}{\Delta t} = \frac{1}{2}\left(\mathbf{A}^*(\delta f + f^*) + \frac{\partial \mathbf{A}^*}{\partial f} f^* \delta f + \mathbf{A}^n f^n\right). \tag{22a}$$

Note that $f^*$ denotes the previous iteration value for $f^{n+\frac{1}{2}}$ in the above equation. The initial value for $f^*$ is $f^n$. The iteration process is converged for the above equation before proceeding to the next equation.

$$\frac{3(\delta f + f^*) - 4f^{n+\frac{1}{2}} + f^n}{\Delta t} = \mathbf{A}^*(\delta f + f^*) + \frac{\partial \mathbf{A}^*}{\partial f} f^* \delta f. \tag{22b}$$

Note that $f^*$ denotes the previous iteration value for $f^{n+1}$ in the above equation. The initial value for $f^*$ is $f^{n+\frac{1}{2}}$.

### 4.2. One-iteration Newton method

Another option is to stop iterating after a single iteration of the converged Newton method:

$$\frac{2\delta f}{\Delta t} = \frac{1}{2}\left(\mathbf{A}^n(\delta f + f^n) + \frac{\partial \mathbf{A}^n}{\partial f} f^n \delta f + \mathbf{A}^n f^n\right). \tag{23a}$$

$$\frac{3\left(\delta f + f^{n+\frac{1}{2}}\right) - 4f^{n+\frac{1}{2}} + f^n}{\Delta t} = \mathbf{A}^{n+1/2}\left(\delta f + f^{n+\frac{1}{2}}\right) + \frac{\partial \mathbf{A}^{n+\frac{1}{2}}}{\partial f} f^{n+\frac{1}{2}} \delta f. \tag{23b}$$

### 4.3. Converged hybrid method

The next variation is to treat the cross sections using Picard's method. This is similar to the Newton method, except that the contribution from the derivatives of the cross sections to the Jacobian are neglected:

$$\frac{2(\delta f + f^* - f^n)}{\Delta t} = \frac{1}{2}\left[\mathbf{B}^*\left(\mathbf{C}^*(\delta f + f^*) + \frac{\partial \mathbf{C}^*}{\partial f} f^* \delta f\right) + \mathbf{B}^n \mathbf{C}^n f^n\right]. \tag{24a}$$

Note that $f^*$ denotes the previous iteration value for $f^{n+\frac{1}{2}}$ in the above equation. The initial value for $f^*$ is $f^n$. The iteration process is converged for the above equation before proceeding to the next.

$$\frac{3(\delta f + f^*) - 4f^{n+\frac{1}{2}} + f^n}{\Delta t} = \mathbf{B}^*\left(\mathbf{C}^*(\delta f + f^*) + \frac{\partial \mathbf{C}^*}{\partial f} f^* \delta f\right). \tag{24b}$$

Note that $f^*$ denotes the previous iteration value for $f^{n+1}$ in the above equation. The initial value for $f^*$ is $f^{n+\frac{1}{2}}$.

It should be noted that the Newton method and the hybrid method converge to the same solution; but the hybrid method will generally be expected to require more iterations to converge.

### 4.4. Two-iteration hybrid method

The last variant is a two-iteration hybrid method. Because Picard's method is used to treat the cross sections, the additional iteration is necessary to achieve second-order accuracy.

$$\frac{2(\delta f)}{\Delta t} = \frac{1}{2}\left[\mathbf{B}^n\left(\mathbf{C}^n(\delta f + f^n) + \frac{\partial \mathbf{C}^n}{\partial f} f^n \delta f\right) + \mathbf{B}^n \mathbf{C}^n f^n\right]. \tag{25a}$$

$$f^* = \delta f + f^n. \tag{25b}$$

$$\frac{2(\delta f + f^* - f^n)}{\Delta t} = \frac{1}{2}\left[\mathbf{B}^*\left(\mathbf{C}^*(\delta f + f^*) + \frac{\partial \mathbf{C}^*}{\partial f} f^* \delta f\right) + \mathbf{B}^n \mathbf{C}^n f^n\right]. \tag{25c}$$

$$f^{n+\frac{1}{2}} = \delta f + f^*. \tag{25d}$$

$$\frac{3\left(\delta f + f^{n+\frac{1}{2}}\right) - 4f^{n+\frac{1}{2}} + f^n}{\Delta t} = \mathbf{B}^{n+\frac{1}{2}}\left(\mathbf{C}^{n+\frac{1}{2}}\left(\delta f + f^{n+\frac{1}{2}}\right) + \frac{\partial \mathbf{C}^{n+\frac{1}{2}}}{\partial f} f^{n+\frac{1}{2}} \delta f\right). \tag{25e}$$

$$f^* = \delta f + f^{n+\frac{1}{2}}. \tag{25f}$$

$$\frac{3(\delta f + f^*) - 4f^{n+\frac{1}{2}} + f^n}{\Delta t} = \mathbf{B}^*\left(\mathbf{C}^*(\delta f + f^*) + \frac{\partial \mathbf{C}^*}{\partial f} f^* \delta f\right). \tag{25g}$$

$$f^{n+1} = \delta f + f^*. \tag{25h}$$

## 5. Computational results

In this section we present our computational results. Two problems are considered and both accuracy and efficiency are measured.

### 5.1. Infinite medium sine wave problem

The first of our test problems is an infinite medium sine wave. Because the solution is infinitely differentiable in space and time, this problem is designed to show asymptotic behavior quickly. The initial radiation energy density is defined as:

$$E(x) = 0.05 + \frac{1 - 0.05}{2}\left[1 + \sin\left\{\frac{\pi}{2}\frac{2x - 0.05}{0.05}\right\}\right], \tag{26}$$

which varies monotonically from 0.05 to 1.0 jerks/cm$^3$. We apply reflective boundary conditions so that our problem represents a continous sine wave in an infinite medium. The temperature is set to be in thermal equilibrium with the material, i.e. $E = aT^4$. As the sine wave evolves toward the final time of 0.02 shakes, it will relax monotonically, approaching a constant solution as $t \to \infty$. The cross sections have the following temperature dependence:

$$\sigma_a(T) = \frac{\sigma_o}{T^3}, \tag{27}$$

where $\sigma_o$ is a constant equal to 0.3, and $\sigma_t(T) = \sigma_a(T)$. The spatial domain is a 0.05 cm thick slab discretized into 50 spatial cells, and the heat capacity, $C_v$, is 0.3 jerks/(cm$^3$ keV). We use fixed time steps and converge the solution to a relative tolerance of $10^{-8}$.

#### 5.1.1. Accuracy

To compare our TR/BDF2 schemes, we run this problem varying the number of time steps from 1 K to 64 K. We compute the error for each method by comparing it with a numerical "exact" solution at the final time of the calculation. This is generated using the converged Newton TR/BDF2 scheme with 1024 K time steps, which is 16 times more refined than the smallest tested time step. The error is computed as:

$$e_{\phi,\Delta t} = \frac{\|\phi_{\Delta t} - \phi_{exact}\|_2}{\|\phi_{exact}\|_2}, \tag{28}$$

where $\phi$ is either $E$ or $T$. For comparison, in addition to the TR/BDF2 based schemes described in Section 4, we include results generated using the Crank–Nicholson scheme. For these two additional methods, we use the converged Newton approach to treat the nonlinearities. Figs. 2 and 3 show the error as a function of the number of time steps for the radiation energy density and material temperature, respectively.

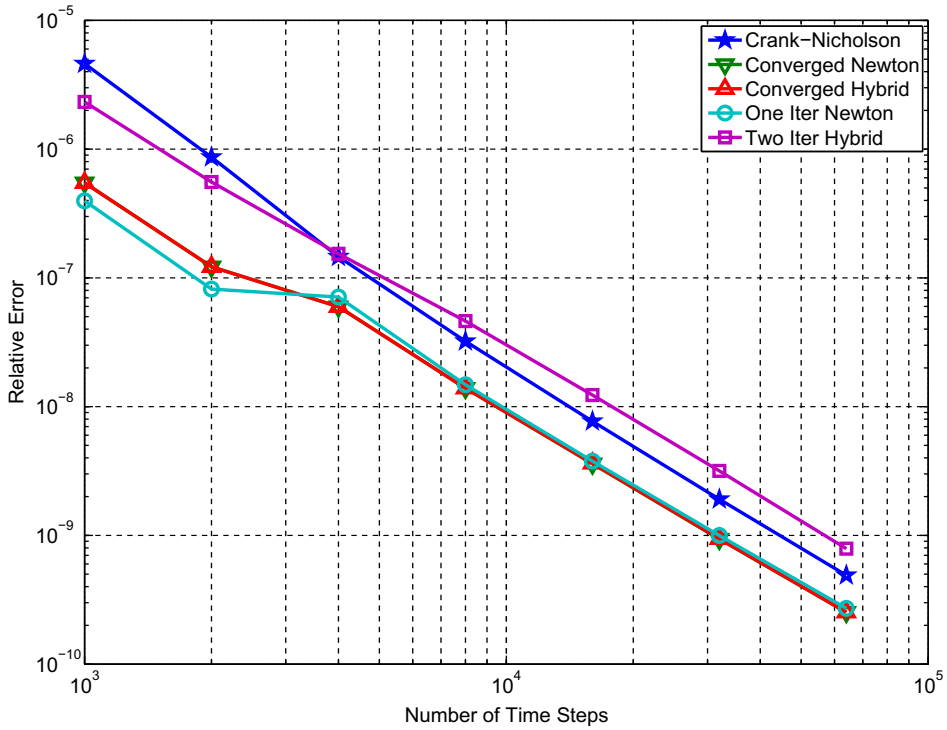


**Fig. 2.** Error in radiation energy density versus number of time steps for the infinite medium sine wave.

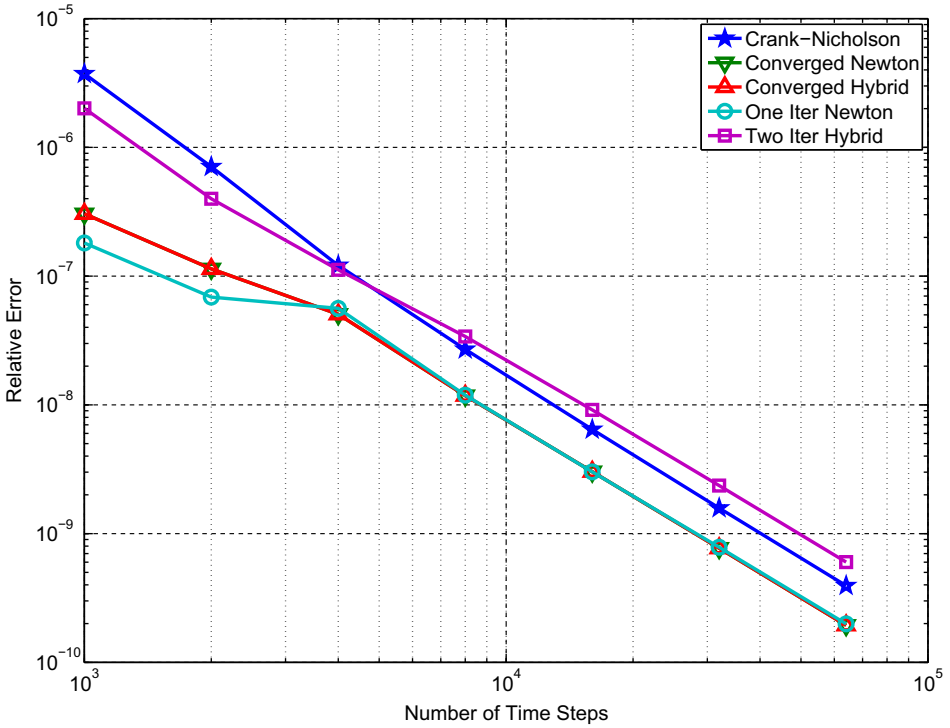


**Fig. 3.** Error in temperature versus number of time steps for the infinite medium sine wave.

**Table 1**
Computed orders of accuracy for the infinite medium sine wave.

| Method | Radiation energy density | Temperature |
|---|---|---|
| Crank–Nicholson | 2.05 | 2.06 |
| Converged Newton TR/BDF2 | 1.97 | 2.00 |
| One-iteration Newton TR/BDF2 | 2.00 | 2.02 |
| Converged hybrid TR/BDF2 | 1.97 | 2.00 |
| Two-iteration hybrid TR/BDF2 | 1.91 | 1.89 |

From these pictures, we can see that the converged TR/BDF2 schemes are the most accurate. Furthermore, as the time step becomes small, the one-iteration Newton method has the same error as the fully converged methods. So, for the infinite medium sine wave problem, as we increase the number of time steps past 4000, one Newton iteration is sufficient to reduce the error associated with convergence below the error of the TR/BDF2 method itself. We can also see that these three TR/BDF2 methods are roughly twice as accurate as the Crank–Nicholson method and six times as accurate as the two-iteration hybrid scheme.

To determine order accuracy, we perform linear-regression analysis on the error data. Table 1 shows the results of this analysis for each method using the portion of the data showing asymptotic behavior.

*5.1.2. Efficiency*

Accuracy is not the only characteristic of interest; we also want to determine the efficiency of each method. We define efficiency as follows:

$$\epsilon_{\phi,\Delta t} = \frac{1}{e_{\phi,\Delta t} W_{\Delta t}}, \tag{29}$$

where $W_{\Delta t}$ is the total number of iterations for the entire calculation, each roughly equivalent to one-iteration of Crank-Nicholson. Thus, the efficiency is a measure of the error reduction per unit work, and the optimal method has the highest efficiency. Figs. 4 and 5 show the efficiencies of the radiation energy density and temperature for the infinite medium sine wave, respectively.

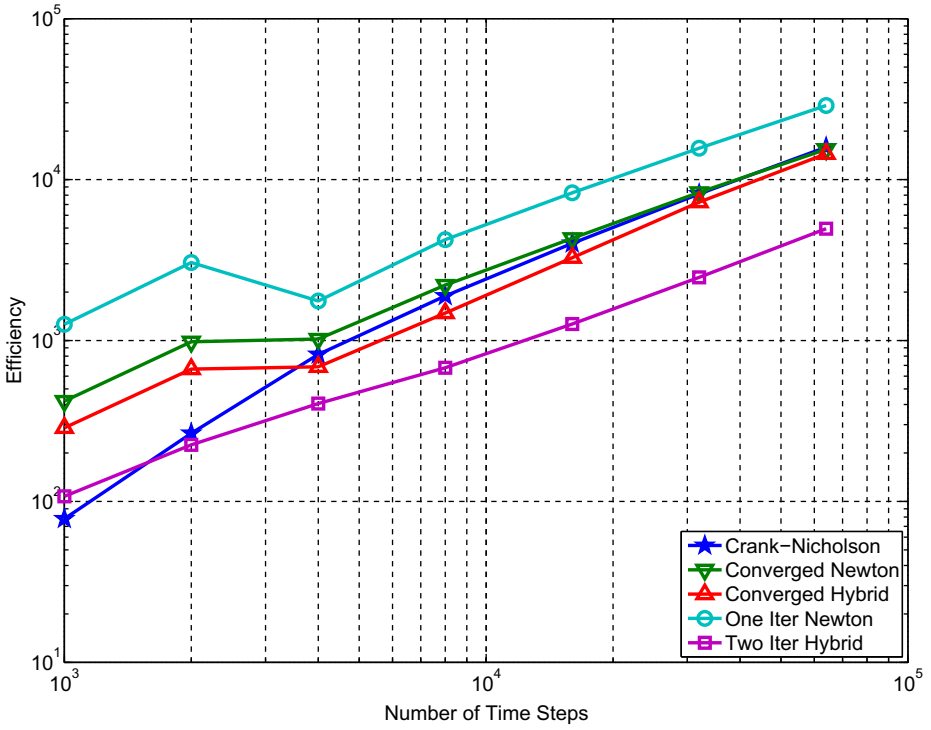


**Fig. 4.** Efficiency for calculating radiation energy density versus number of time steps for the infinite medium sine wave.

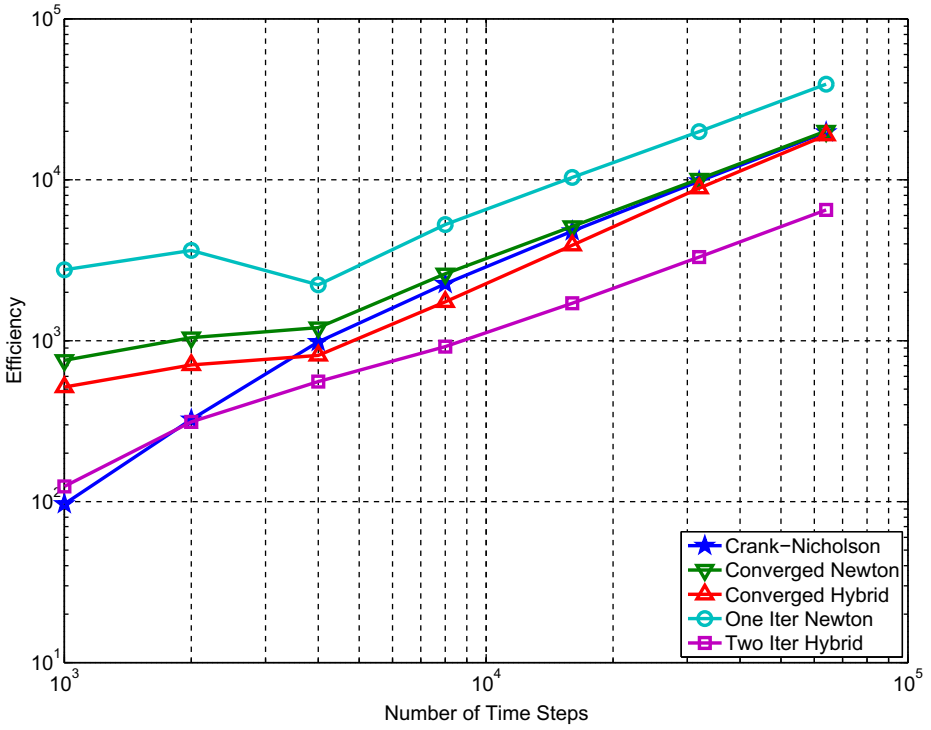


**Fig. 5.** Efficiency for calculating temperature versus number of time steps for the infinite medium sine wave.

In each of these figures, we can see that the one-iteration Newton scheme is twice as efficient as the converged schemes. Moreover, it is roughly an order of magnitude more efficient than the two-iteration hybrid scheme.

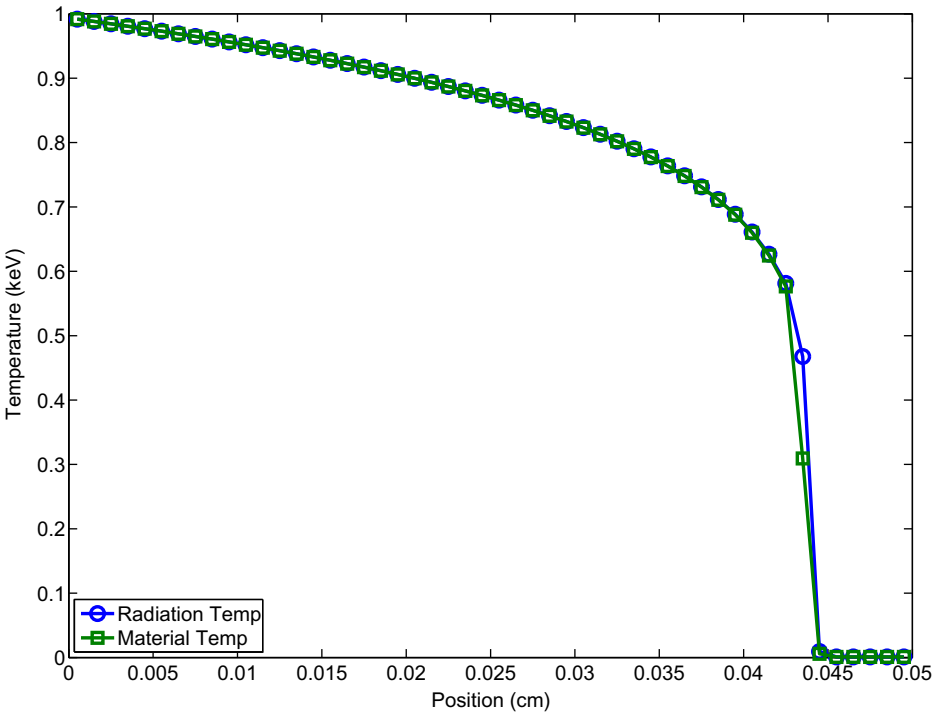


**Fig. 6.** Final solution of Marshak wave problem.

### 5.2. Marshak wave

The next test is a Marshak wave, which is designed to compare the methods using a more realistic problem. Here, we use a constant initial temperature of 0.001 keV throughout the interior of the problem with a 1 keV source at the left boundary. The right boundary is a vacuum, and again, the radiation energy density and material temperature are in thermal equilibrium. $t_{fin}$ is 0.1 shake, and $\sigma_o = 300$. Fig. 6 shows the radiation and material temperatures at the final time, where the radiation temperature is defined as:

$$T_R = \sqrt[4]{E/a}. \tag{30}$$

#### 5.2.1. Time step control

For this problem, we use a variable time step control scheme based on a user-specified "target temperature change", $\Delta T_{targ}$. For a given time step, the maximum relative change is computed using:

$$\Delta T = 2 \max_i \frac{|T_i^{n+1} - T_i^n|}{T_i^{n+1} + T_i^n}. \tag{31}$$

This result is compared with the target temperature change to determine the next time step:

$$\Delta t^{n+1/2} = \min\left(\frac{\Delta T_{targ}}{\Delta T}\Delta t^{n-1/2}, t - t_{fin}\right). \tag{32}$$

The second term forces the final time step to end the calculation at $t_{fin}$. Also, in order to ensure that the temperature doesn't vary too much, $\Delta T$ is also compared with a maximum allowed temperature change, $\Delta T_{max}$. If $\Delta T > \Delta T_{max}$, then the time step $\Delta t^{n+1/2}$ is reduced by a factor of 1/3, and the calculation is repeated from $t_n$. In our calculations, we set $\Delta T_{max} = 1.2\Delta T_{targ}$.

#### 5.2.2. Accuracy

We run this problem varying the target temperature change from 1% to 20% and converging the solution to a relative tolerance of $10^{-4}$. The exact solution is computed using one million fixed time steps, i.e. $\Delta t_{exact} = 10^{-7}$ shakes, which is the minimum time step allowed in our calculations. The exact solution uses roughly 30 times more time steps than the 1% target calculation. Figs. 7 and 8 show the error in radiation energy density and temperature, respectively, for the Marshak wave.

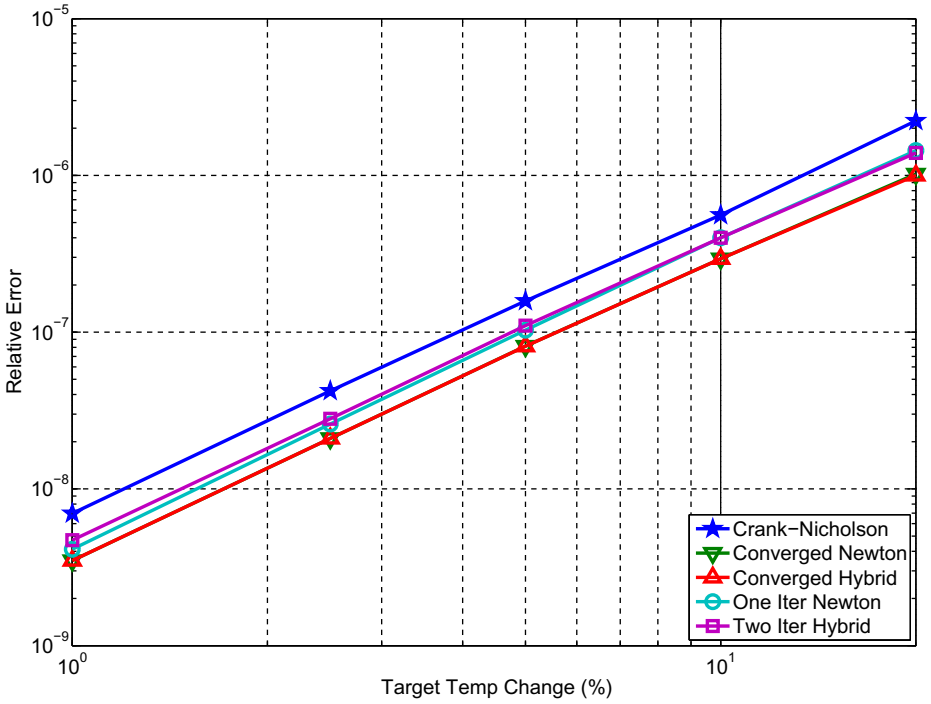


**Fig. 7.** Error in radiation energy density versus number of time steps for the Marshak wave.

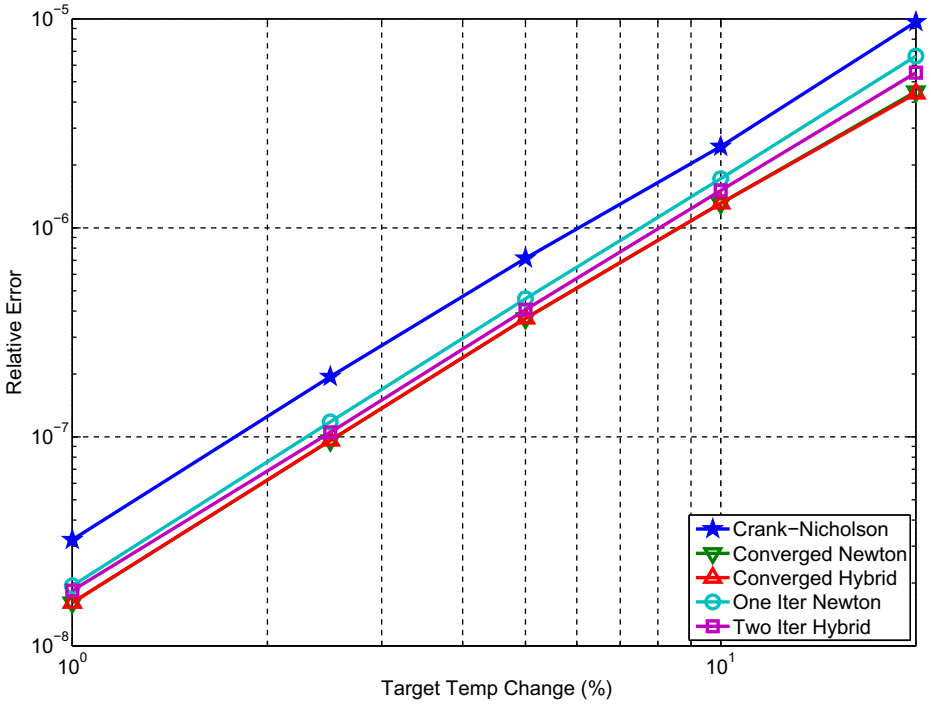


**Fig. 8.** Error in temperature versus number of time steps for the Marshak wave.

Again, we see that the converged TR/BDF2 schemes are the most accurate by about a factor of 2. Furthermore, because the one-iteration scheme is never quite as accurate as the converged schemes, we see some benefit to converging the nonlinear terms in this problem. Though this problem has discontinuities, we still see asymptotic behavior in the error allowing us to compute the order-accuracy of each method, shown in Table 2.

**Table 2**
Computed orders of accuracy for the Marshak wave.

| Method | Radiation energy density | Temperature |
|---|---|---|
| Crank–Nicholson | 1.93 | 1.91 |
| Converged Newton TR/BDF2 | 1.92 | 1.90 |
| One-iteration Newton TR/BDF2 | 1.98 | 1.97 |
| Converged hybrid TR/BDF2 | 1.92 | 1.90 |
| Two-iteration hybrid TR/BDF2 | 1.92 | 1.93 |

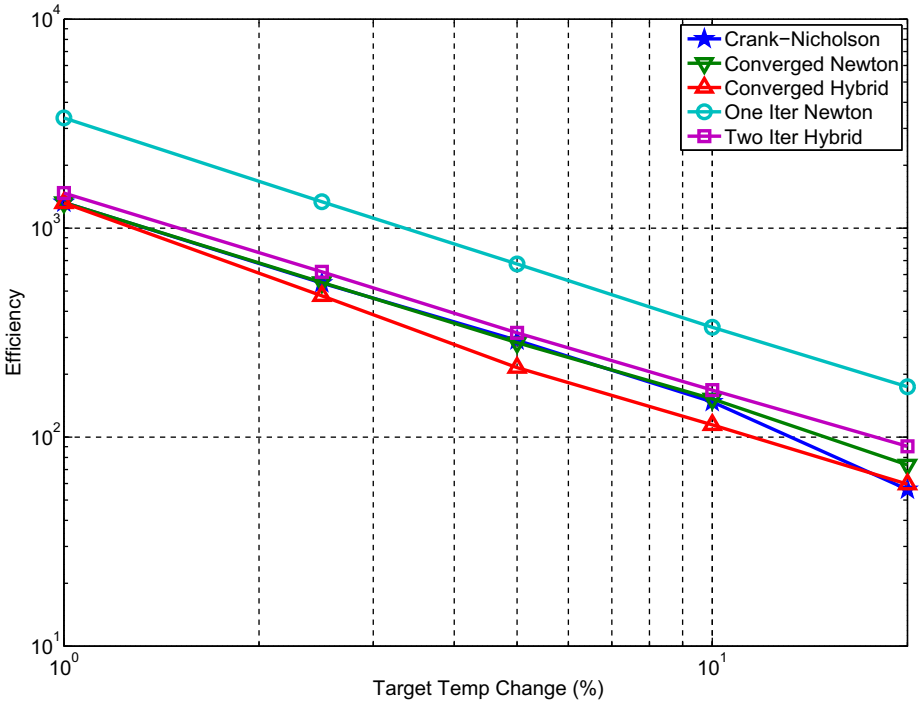


**Fig. 9.** Efficiency for calculating radiation energy density versus number of time steps for the Marshak wave.

*5.2.3. Efficiency*

As with the infinite medium sine problem, we also compare the efficiencies of each method for the Marshak wave. Figs. 9 and 10 show these efficiencies for radiation energy and material temperature.

From these figures we can see that the one-iteration Newton method is, again, twice as efficient as any other scheme. In this case, however, the two-iteration hybrid method is also more efficient than the converged schemes. This is a result of the extra effort required to converge the nonlinear terms when the solution is discontinuous.

*5.3. The maximum principle*

There is one advantage to fully converging the nonlinearities that we have not discussed because it did not arise in our test problems. This relates to the preservation of the thermodynamic maximum principle. This principle is quite simple and can be characterized as follows. Given a closed thermodynamic system with an initial temperature distribution and no inhomogeneous or external energy sources, the temperature must evolve such that the temperature at any point never exceeds the maximum initial temperature in the system. It has been observed that this principle can be violated with sufficiently large time steps if the nonlinearities are not converged [10]. To our knowledge, this effect has not been theoretically analyzed except in case of the implicit Monte Carlo method where the nonlinearities are never converged [11]. For example, in the Marshak wave problem, neither the radiation temperature nor the material temperature should exceed the boundary radiation temperature of 1 keV. We performed the Marshak problem with a fixed time step of $2 \times 10^{-4}$ sh using both the one-iteration Newton method and the converged Newton method. The material temperature solutions after two time steps

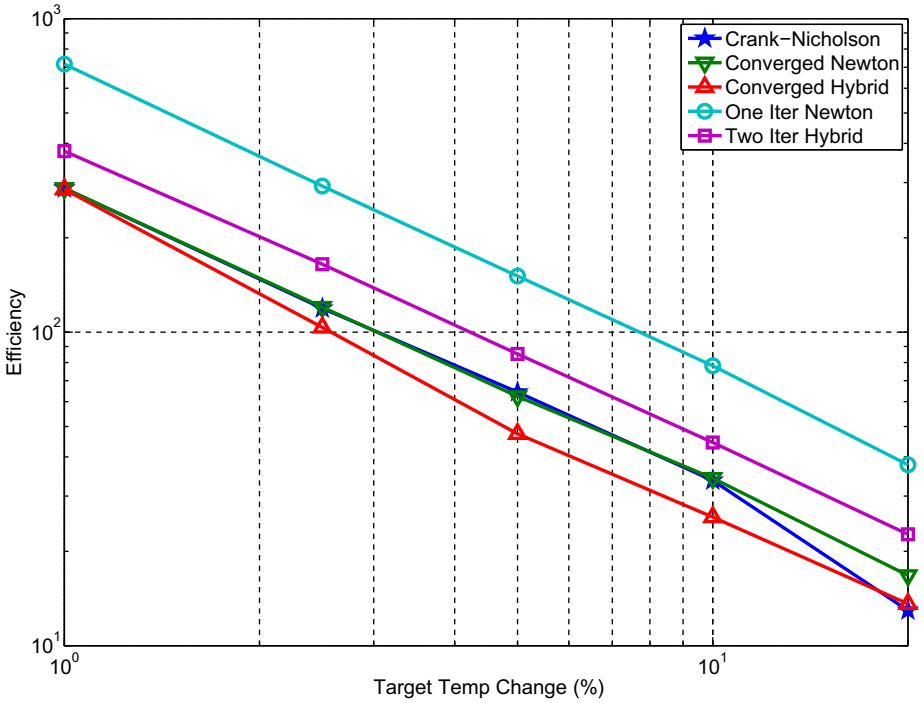


**Fig. 10.** Efficiency for calculating temperature as a function of times teps for the Marshak wave.

are compared for these two methods in Fig. 11. The one-iteration Newton solution clearly violates the maximum principle, but the converged Newton solution does not. This effect does not appear when our time step control algorithm is used, presumably because the time steps are sufficiently small to avoid it. Nonetheless this is an effect that should generally be kept in mind when choosing a time-integration scheme.

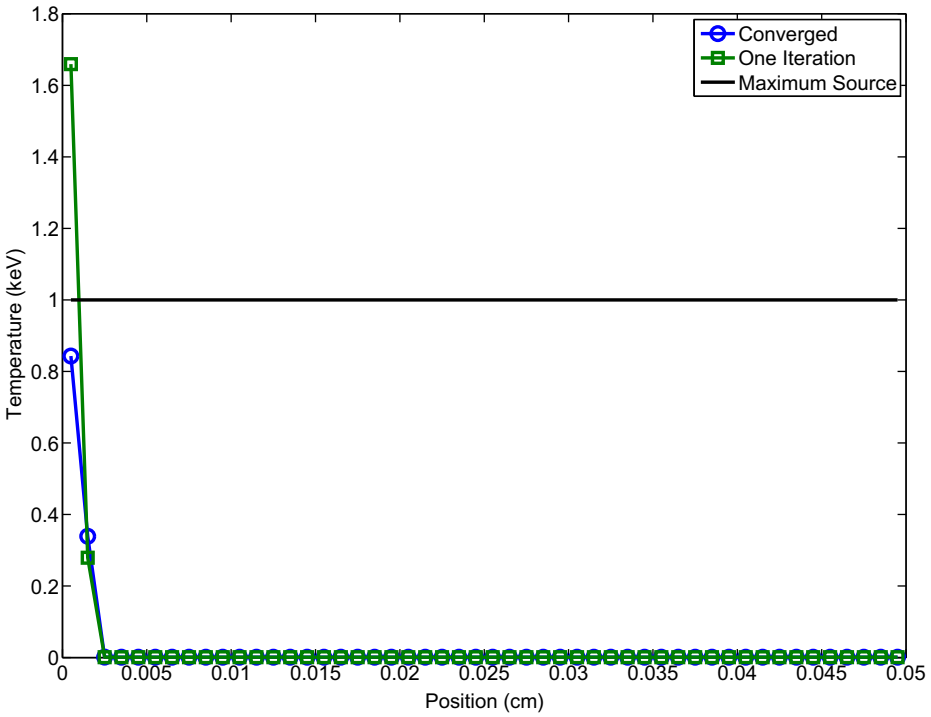


**Fig. 11.** Material temperature solutions after two time steps for the Marshak wave problem with fixed time steps of $2 \times 10^{-4}$ sh.

## 6. Conclusions

The TR/BDF2 method meets the qualifications that we outlined, and thus appears to be a valuable alternative to existing schemes. In each of the test problems, we find that the converged TR/BDF2 schemes are consistently the most accurate, and the one-iteration Newton TR/BDF2 scheme is always the most efficient. This result is in basic agreement with [3], which also shows the one-iteration Newton variant to be the most efficient treatment of the nonlinear terms. We can see that the cost of neglecting the temperature derivatives of the cross sections can reduce efficiency by at least one half and as much as an order of magnitude.

For the smooth test problem, the converged hybrid method is not only more accurate but is also more efficient than its fixed iteration alternative. However, for the Marshak wave problem, the two-iteration hybrid scheme has superior efficiency to both the converged Newton and hybrid schemes. The test problems we considered are certainly not exhaustive. Our results indicate that it is possible for the relative performance of the various methods to change from one type of problem to another. We suspect that if maximum efficiency is desired for any given temporal discretization, one should write computer programs with options for both a fixed number of iterations and full convergence of the nonlinearities. As previously noted, preserving the maximum principle independent of time step requires converging the nonlinearities.

In future work, we intend to explore ways of mitigating the absence of the cross-section derivatives using some form of approximate derivatives. We also intend to develop an IMEX based, second-order radiation hydrodynamics algorithm using TR/BDF2 for the radiation.

## Acknowledgment

We thank Professor Jean Ragusa of Texas A&M University for many invaluable discussions relating to Runge–Kutta methods and time-integration in general. Work by Edwards and Morel was partially supported by the Predictive Sciences Academic Alliances Program in DOE NNSA-ASC under Grant DE-FC52-08NA28616.

## Appendix A. Spatial discretization

In discretizing the radiative transfer equations in space, we want to preserve second-order accuracy for the radiation energy density, radiation energy flux, and material temperature. To accomplish this, we apply a linear-discontinous Galerkin approximation. Since such a method cannot be applied directly to a second-order equation, we begin the derivation of our discrete equations by re-writing the diffusion equation in first-order form. In particular, Eqs. (1) and (2) are expressed as follows:

$$\frac{\partial E}{\partial t}+\frac{\partial F}{\partial x}=\sigma_a c(aT^4-E), \tag{A.1}$$

$$\frac{c}{3}\frac{\partial E}{\partial x}+\sigma_t F=0, \tag{A.2}$$

$$C_v\frac{\partial T}{\partial t}=\sigma_a c(E-aT^4). \tag{A.3}$$

We divide the spatial domain into a 1D mesh with constant cell spacing where cell "$i$" is defined as $x=\{x{:}x\in(x_{i-1/2},x_{i+1/2})\}$, and

$$\Delta x=x_{i+1/2}-x_{i-1/2}, \tag{A.4}$$

Because the shape of the exact solution is unknown, we approximate the solution in each cell using a linear representation. To accomplish this, we first define a set of linear basis functions. We use a set of tent functions as our basis, each of which has a value of 1 at a given vertex and 0 at all the other vertices. So, for a given cell, the two non-zero basis functions in that cell may be defined as:

$$b_L(x)=\frac{x_{i+1/2}-x}{x_{i+1/2}-x_{i-1/2}}, \tag{A.5a}$$

$$b_R(x)=\frac{x-x_{i-1/2}}{x_{i+1/2}-x_{i-1/2}}. \tag{A.5b}$$

Using these basis functions, we define the radiation energy density, radiation energy flux, and material temperature inside a given cell $i$ as:

$$E(x)=E_L b_L+E_R b_R, \tag{A.6a}$$

$$F(x)=F_L b_L+F_R b_R, \tag{A.6b}$$

$$T(x)=T_L b_L+T_R b_R. \tag{A.6c}$$

Furthermore, we allow the solution to be discontinous at cell interfaces so that, for example, $E_{R,i-1}$ may not necessarily be equal to $E_{L,i}$. This overall approach is called a linearly discontinuous Galerkin method and is very similar to the method described by Reed and Hill to discretize the steady-state $S_2$ neutron transport equation [12].

We obtain the weak form of the solution to the balance equation by multiplying (A.1) by a generic test function and integrating over the width of the cell, yielding:

$$\int_{x_{i-1/2}}^{x_{i+1/2}} b_k \frac{\partial E}{\partial t}\,dx + \int_{x_{i-1/2}}^{x_{i+1/2}} b_k \frac{\partial F}{\partial x}\,dx = \int_{x_{i-1/2}}^{x_{i+1/2}} b_k \sigma_a c(aT^4 - E)\,dx. \tag{A.7}$$

Then, using integration by parts, we have:

$$\int_{x_{i-1/2}}^{x_{i+1/2}} b_k \frac{\partial E}{\partial t}dx + \left[(b_k F)|_{x=x_{i+1/2}} - (b_k F)|_{x=x_{i-1/2}} - \int_{x_{i-1/2}}^{x_{i+1/2}} F\frac{\partial b_k}{\partial x}\,dx\right] = \int_{x_{i-1/2}}^{x_{i+1/2}} b_k \sigma_a c\Big(aT^4 - E\Big)dx. \tag{A.8}$$

Using a similar process with (A.2), we derive the weak form of the solution for the radiation energy flux:

$$\frac{c}{3}\left[(b_k E)|_{x=x_{i+1/2}} - (b_k E)|_{x=x_{i-1/2}} - \int_{x_{i-1/2}}^{x_{i+1/2}} E\frac{\partial b_k}{\partial x}\,dx\right] + \int_{x_{i-1/2}}^{x_{i+1/2}} b_k \sigma_t F\,dx = 0. \tag{A.9}$$

At this point we need expressions relating $E_{i-1/2}$ and $F_{i-1/2}$, the edge values of $E$ and $F$, respectively, to interior values. These relationships are obtained via the characteristic variables:

$$\epsilon^+ = \frac{c}{2}E + \frac{\sqrt{3}}{2}F \tag{A.10a}$$

and

$$\epsilon^- = \frac{c}{2}E - \frac{\sqrt{3}}{2}F. \tag{A.10b}$$

The first characteristic variable, $\epsilon^+$ represents an angular radiation intensity that propagates from left to right, while the second characteristic variable, $\epsilon^-$ represents an angular radiation intensity that propagates from right to left. These characteristic variables are defined at the cell edges via upwinding:

$$\epsilon^+_{i-1/2} = \frac{c}{2}E_{R,i-1} + \frac{\sqrt{3}}{2}F_{R,i-1}, \tag{A.11a}$$

$$\epsilon^-_{i-1/2} = \frac{c}{2}E_{L,i} - \frac{\sqrt{3}}{2}F_{L,i}. \tag{A.11b}$$

Using the above definitions, we can determine the edge values $E_{i-1/2}$ and $F_{i-1/2}$ as follows:

$$\begin{aligned} E_{i-1/2} &= \frac{1}{c}\left(\epsilon^+_{i-1/2} + \epsilon^-_{i-1/2}\right), \\ &= \frac{E_{L,i} + E_{R,i-1}}{2} + \frac{\sqrt{3}}{2c}(F_{R,i-1} - F_{L,i}), \end{aligned} \tag{A.12}$$

$$\begin{aligned} F_{i-1/2} &= \frac{1}{\sqrt{3}}\epsilon^+_{i-1/2} + \frac{-1}{\sqrt{3}}\epsilon^-_{i-1/2}, \\ &= \frac{cE_{R,i-1} - cE_{L,i}}{2\sqrt{3}} + \frac{1}{2}(F_{R,i-1} + F_{L,i}). \end{aligned} \tag{A.13}$$

Because we have 2 equations and 4 unknowns describing the radiation, we can fully determine the system by using both $b_L$ and $b_R$ as test functions in (A.8) and (A.9). We will also use a process called "mass matrix lumping." To explain this, consider the integral of the time derivative term using both the left and right basis functions. Writing this in matrix form, we have:

$$\begin{bmatrix} \int_{x_{i-1/2}}^{x_{i+1/2}} b_L b_L\,dx & \int_{x_{i-1/2}}^{x_{i+1/2}} b_L b_R\,dx \\ \int_{x_{i-1/2}}^{x_{i+1/2}} b_R b_L\,dx & \int_{x_{i-1/2}}^{x_{i+1/2}} b_R b_R\,dx \end{bmatrix} \begin{bmatrix} \frac{\partial E_L}{\partial t} \\ \frac{\partial E_R}{\partial t} \end{bmatrix} = \Delta x \begin{bmatrix} \frac{1}{3} & \frac{1}{6} \\ \frac{1}{6} & \frac{1}{3} \end{bmatrix} \begin{bmatrix} \frac{\partial E_L}{\partial t} \\ \frac{\partial E_R}{\partial t} \end{bmatrix}. \tag{A.14}$$

The matrix on the right-hand side of (A.14) is called a "mass matrix" because it does not involve integrals over the spatial derivatives. In mass matrix lumping, the diagonal of each row is set equal to the sum of the elements of the row, and the off-diagonals are set to zero. For (A.14), this becomes:

$$\Delta x \begin{bmatrix} \frac{1}{3} & \frac{1}{6} \\ \frac{1}{6} & \frac{1}{3} \end{bmatrix} \begin{bmatrix} \frac{\partial E_L}{\partial t} \\ \frac{\partial E_R}{\partial t} \end{bmatrix} \Rightarrow \Delta x \begin{bmatrix} \frac{1}{2} & 0 \\ 0 & \frac{1}{2} \end{bmatrix} \begin{bmatrix} \frac{\partial E_L}{\partial t} \\ \frac{\partial E_R}{\partial t} \end{bmatrix}. \tag{A.15}$$

Integrating (A.8) and (A.9) using $b_k = b_L$ and incorporating mass matrix lumping, we have:

$$\frac{\Delta x}{2}\frac{\partial E_{L,i}}{\partial t}+\frac{c}{2\sqrt{3}}(E_{L,i}-E_{R,i-1})+\frac{F_{R,i}-F_{R,i-1}}{2}=\frac{\Delta x}{2}\sigma_{a,L,i}c\left(aT_{L,i}^4-E_{L,i}\right), \tag{A.16}$$

$$\frac{cE_{R,i}-cE_{R,i-1}}{6}-\frac{F_{R,i-1}}{2\sqrt{3}}+\left(\frac{\sigma_{t,L,i}\Delta x}{2}+\frac{1}{2\sqrt{3}}\right)F_{L,i}=0. \tag{A.17}$$

Likewise, integrating (A.8) and (A.9) using $b_k = b_R$, we have:

$$\frac{\Delta x}{2}\frac{\partial E_{R,i}}{\partial t}+\frac{c}{2\sqrt{3}}(E_{R,i}-E_{L,i+1})+\frac{F_{L,i+1}-F_{L,i}}{2}=\frac{\Delta x}{2}\sigma_{a,R,i}c\left(aT_{R,i}^4-E_{R,i}\right), \tag{A.18}$$

$$\frac{cE_{L,i+1}-cE_{L,i}}{6}-\frac{F_{L,i+1}}{2\sqrt{3}}+\left(\frac{\sigma_{t,L,i}\Delta x}{2}+\frac{1}{2\sqrt{3}}\right)F_{L,i}=0. \tag{A.19}$$

We obtain equations for the temperature unknowns in a similar manner, by multiplying (A.3) by a basis function and integrating over the cell width as:

$$\int_{x_{i-1/2}}^{x_{i+1/2}} C_v b_k\frac{\partial T}{\partial t}\,dx=\int_{x_{i-1/2}}^{x_{i+1/2}} b_k\sigma_a c\left(E-aT^4\right)dx. \tag{A.20}$$

where $k = L, R$. Carrying out this integration and using mass matrix lumping, we get:

$$C_v\frac{\partial T_{k,i}}{\partial t}=\sigma_{a,k,i}c\left(E_{k,i}-aT_{k,i}^4\right). \tag{A.21}$$

Here, we have a point-wise expression for the temperature unknowns. This preserves the spatial independence of (A.3). Next, we consider the solution at the left and right boundaries.

In our problems, we use source, vacuum, and reflective boundary conditions. Boundary conditions are met by appropriately defining the incident characteristic variables at the boundries:

$$\epsilon_{1/2}^{+}=\frac{c}{2}E_L^{inc}+\frac{\sqrt{3}}{2}F_L^{inc}, \tag{A.22}$$

$$\epsilon_{N+1/2}^{-}=\frac{c}{2}E_R^{inc}-\frac{\sqrt{3}}{2}F_R^{inc}, \tag{A.23}$$

where $E_L^{inc}$, $E_R^{inc}$, $F_L^{inc}$, and $F_R^{inc}$ represent the incident values for the left and right values of the radiation energy density and radiation energy flux. To obtain vacuum boundary conditions, one need only set the incident characteristic variables to zero. This uniquely defines both the incident $E$ and $F$ to be identically zero. For a black-body source condition the incident characteristic variables are set to the correct incident intensity, $acT_{inc}^4/2$, where $T_{inc.}$ is the black-body temperature. For example, consider a left boundary black-body source. The characteristic variable is set as follows:

$$\epsilon_{1/2}^{+}=\frac{c}{2}E_L^{inc}+\frac{\sqrt{3}}{2}F_L^{inc}=\frac{1}{2}acT_{inc}^4. \tag{A.24}$$

Thus, we have two parameters available, $E_L^{inc}$ and $F_L^{inc}$, to determine one value of the incident characteristic variable. For simplicity, we simply choose to set $F_L^{inc}$ to zero and set $E_L^{inc}=aT_{inc}^4$.

Substituting (A.22) into (A.12) and (A.13), we obtain equations for the radiation energy density and energy flux at the left boundary:

$$\frac{\Delta x}{2}\frac{\partial E_L,1}{\partial t}+\frac{c}{2\sqrt{3}}E_{L,1}+\frac{F_{R,1}}{2}=\frac{\Delta x}{2}\sigma_{a,L,1}c(aT_{L,1}^4-E_{L,1})+\frac{cE_L^{inc}}{2\sqrt{3}}+\frac{F_L^{inc}}{2}, \tag{A.25}$$

$$\frac{cE_{R,1}}{6}+\left(\frac{\sigma_{t,L,1}\Delta x}{2}+\frac{1}{2\sqrt{3}}\right)F_{L,1}=\frac{cE_L^{inc}}{6}+\frac{F_L^{inc}}{2\sqrt{3}}. \tag{A.26}$$

Similarly, substituting (A.23) into (A.12) and (A.13), we obtain equations for the solution at the right boundary:

$$\frac{\Delta x}{2}\frac{\partial E_R,N}{\partial t}+\frac{c}{2\sqrt{3}}E_{R,N}-\frac{F_{L,N}}{2}=\frac{\Delta x}{2}\sigma_{a,R,N}c\left(aT_{R,N}^4-E_{R,N}\right)+\frac{cE_R^{inc}}{2\sqrt{3}}-\frac{F_R^{inc}}{2}, \tag{A.27}$$

$$-\frac{cE_{L,N}}{6}+\left(\frac{\sigma_{t,R,N}\Delta x}{2}+\frac{1}{2\sqrt{3}}\right)F_{R,N}=-\frac{cE_R^{inc}}{6}+\frac{F_L^{inc}}{2\sqrt{3}}. \tag{A.28}$$

Here, we note that (A.21) does not require boundary conditions. Finally, we satisfy reflective conditions by equating the incoming and outgoing characteristic variables at the boundary

$$\epsilon^{-}=\epsilon^{+}. \tag{A.29}$$

So, for a reflective condition, this means that:

$$E_{1/2} = \frac{2}{c}\epsilon^{-}_{1/2} = \frac{c}{2}E_{L,1} - \frac{\sqrt{3}}{2}F_{L,1}, \tag{A.30a}$$

$$E_{N+1/2} = \frac{2}{c}\epsilon^{+}_{1/2} = \frac{c}{2}E_{R,N} + \frac{\sqrt{3}}{2}F_{R,N}, \tag{A.30b}$$

$$F_{1/2} = F_{N+1/2} = 0. \tag{A.30c}$$

Plugging (A.30a) and (A.30c) into (A.12) and (A.13) for the left energy density and energy flux in the first cell, we have the following equations for a left reflective boundary condition:

$$\frac{\Delta x}{2}\frac{\partial E_{L,1/2}}{\partial t} + \frac{F_{L,1/2} + F_{R,1/2}}{2} = c\sigma_{a,L,1/2}\left(aT^4_{L,1/2} - E_{L,1/2}\right) \tag{A.31}$$

$$\frac{c}{3}\left(\frac{E_{R,1} - E_{L,1}}{2}\right) + \left(\frac{\Delta x}{2}\sigma_{t,L,1} + \frac{1}{\sqrt{3}}\right)F_{L,1} = 0 \tag{A.32}$$

Likewise, for a right reflective boundary, we have the following for the right energy density and energy flux in the last cell:

$$\frac{\Delta x}{2}\frac{\partial E_{R,N+1/2}}{\partial t} + \frac{F_{L,N+1/2} + F_{R,N+1/2}}{2} = c\sigma_{a,R,N+1/2}\left(aT^4_{R,N+1/2} - E_{R,N+1/2}\right), \tag{A.33}$$

$$\frac{c}{3}\left(\frac{E_{R,N} - E_{L,N}}{2}\right) + \left(\frac{\Delta x}{2}\sigma_{t,R,N} + \frac{1}{\sqrt{3}}\right)F_{R,N} = 0. \tag{A.34}$$

## References


[1] E. Hairer, G. Wanner, Solving ordinary differential equations II, Second Revised ed., Springer Series in Computational Mathematics, Springer, New York, 2002.

[2] T.A. Wareing, J.E. Morel, J.M. McGhee, A diffusion synthetic acceleration method for the SN equations with discontinuous finite element space and time differencing, in: Proceedings of the International Conference on Mathematics and Computation, Reactor Physics and Environmental Analyses in Nuclear Applications, Madrid, Spain, September 27–30, vol. 1, 1999, pp. 45–54.

[3] Robert B. Lowrie, A comparison of implicit time integration methods for nonlinear relaxation and diffusion, J. Comput. Phys. 196 (2004) 566–590.

[4] J.S. Warsa, T.A. Wareing, J.E. Morel, Fully consistent diffusion synthetic acceleration of linear discontinuous transport discretizations on three-dimensional unstructured meshes, Nucl. Sci. Eng. 141 (2002) 236–251.

[5] J.S. Warsa, T.A. Wareing, J.E. Morel, Solution of the discontinuous $P_1$ equations in two-dimensional cartesian geometry with two-level preconditioning, SIAM J. Sci. Comput. 24 (2003) 2093–2124.

[6] R.E. Bank, W.M. Coughran Jr., W. Fichtner, E.H. Grosse, D.J. Rose, R.K. Smith, Transient simulation of silicon devices and circuits, IEEE Trans. Comput. Aided Des. 4 (4) (1985) 436–451.

[7] J.C. Butcher, Numerical Methods for Ordinary Differential Equations, John Wiley & Sons Ltd, Chichester, England, 2008.

[8] D.A. Knoll, D.E. Keyes, Jacobian-free NewtonKrylov methods: a survey of approaches and applications, J. Comput. Phys. 193 (2004) 357–397.

[9] J. Stoer, J. Bulirsch, Introduction to Numerical Analysis, third ed., Springer, New York, 2002.

[10] D.A. Knoll, R.B. Lowrie, J.E. Morel, Numerical analysis of time-integration errors for non-equilibrium radiation diffusion, J. Comput. Phys. 226 (2007) 1332–1347.

[11] E.W. Larsen, B. Mercier, Analysis of a Monte Carlo method for nonlinear radiative transfer, J. Comput. Phys. 71 (1987) 50–64.

[12] W.H. Reed, T.R. Hill, "Triangular Mesh Methods for the Neutron Transport Equation," Technical Report LA-UR-73-479, Los Alamos Scientific Laboratory, 1973.